

# The Impact of Melt-Conditioned Twin-Roll Casting on the Downstream Processing of an AZ31 Magnesium Alloy

I. BAYANDORIAN, Y. HUANG, Z. FAN, S. PAWAR, X. ZHOU, and G.E. THOMPSON

Melt conditioning by intensive shear was used prior to twin-roll casting of AZ31 magnesium alloy strip to promote heterogeneous nucleation and to provide a refined and uniform microstructure without severe macrosegregation. The cast strip was then processed by homogenization, hot rolling, and annealing, and its downstream processing was compared with a similar cast strip produced without melt conditioning. Melt conditioning produced strip with accelerated kinetics of recrystallization during homogenization and improved performance in hot rolling and improved tensile properties. An average tensile elongation of ~28 pct was achieved, which is substantially higher than the ~9 pct obtained for the strip produced without melt conditioning which is consistent with reported values (~6 pct to 16 pct). The as-cast, homogenized, and hot-rolled microstructures of the strip were characterized. The kinetics of homogenization and hot-rolling process have been discussed in detail.

DOI: 10.1007/s11661-011-1006-3

© The Minerals, Metals & Materials Society and ASM International 2011

## I. INTRODUCTION

WROUGHT magnesium alloys in sheet form are of interest for applications in the automotive and electronic industries because of their low density, outstanding electromagnetic shielding capability, and excellent heat dissipation.<sup>[1,2]</sup> However, their production is inefficient and expensive because of low ductility. Grain refinement in magnesium alloys enhances strength and improves ductility by promoting the operation of nonbasal slip systems<sup>[3,4]</sup> and restricting twinning.<sup>[5-7]</sup> Several procedures have been developed to produce fine-grain structures in magnesium alloys, including powder metallurgy,<sup>[8]</sup> rapid solidification,<sup>[9]</sup> and severe plastic deformation,<sup>[10-12]</sup> but only small quantities of material can be obtained from these process routes. Although thermomechanical processing through repetitive hot/warm rolling/extrusion of ingot slabs combined with heat treatment can produce well-refined microstructures,<sup>[13-15]</sup> it is extremely costly and has an adverse effect on the anisotropy and ductility as strong basal texture develops.<sup>[14,16,17]</sup>

Twin-roll casting can produce a magnesium alloy strip directly from the melt with a thickness less than 6 mm, eliminating the need for the use of a breakdown mill and most of the passes in the finishing mill that are required in conventional processing.<sup>[18]</sup> Twin-roll casting offers both significant cost savings and the potential to

improve strip quality by refining grain size based on the higher cooling rate compared with the conventional ingot casting. Another benefit of producing magnesium alloy strip by this route is the possibility of providing a weak or even random texture if the process is controlled to require only a minimum of plastic deformation. Many reports showed that the solidification rate achieved by twin-roll casting can improve alloy properties by homogenizing microstructure, refining grain size, and reducing segregation, *etc.*<sup>[19-21]</sup> However, the quality of magnesium alloy strip produced by the existing twin roll casting techniques is still limited by the formation of columnar dendrite grains and centerline segregation.<sup>[22-24]</sup> Optimizing the process and developing alloys that better suit the process can help resolve these problems in conjunction with effective grain refinement at the solidification stage.

The addition of a grain refiner works well for most alloy casting processes. However, there are potential problems with inoculation of grain refiners in twin-roll casting such as nozzle blockage and upstream nucleation,<sup>[20]</sup> and potentially the impairment of the mechanical properties and the recyclability of the final product.<sup>[24,25]</sup> Most importantly, effective grain refiners are still sought for magnesium alloys with aluminum additions such as the AZ and AK series, although proven chemical refiner additions, *e.g.*, zirconium, are available for aluminum-free magnesium alloys.<sup>[26,27]</sup> Electromagnetic fields can be used to modify material convection in the solidification zone, but this process is difficult to control.<sup>[28]</sup> Physical melt treatment is an alternative option and melt conditioning by intensive shear prior to solidification has been developed for this purpose.<sup>[24,29,30]</sup> This technique has been applied successfully for both aluminum and magnesium alloys prior to casting by a range of casting methods,<sup>[31-33]</sup> and it has proved to be particularly effective for the solidification processing of magnesium alloys.<sup>[24,29,34]</sup>

---

I. BAYANDORIAN, Research Fellow, Y. HUANG, Lecturer, and Z. FAN, Professor, are with the EPSRC Centre for Innovative Manufacturing in Liquid Metal Engineering and BCAST, Brunel University, Uxbridge, Middlesex UB8 3PH, United Kingdom. Contact e-mail: yan.huang@brunel.ac.uk S. PAWAR, Research Student, X. ZHOU, Reader, and G.E. THOMPSON, Professor, are with the Corrosion and Protection Centre, School of Materials, University of Manchester, Manchester M13 9PL, United Kingdom.

Manuscript submitted September 28, 2010.

Article published online November 19, 2011

Magnesium alloy strip produced by conventional twin-roll casting requires additional processing including homogenization, rolling, and annealing. Because of the thickness of constraints associated with twin-roll casting, the possibility of modifying the as-cast microstructures and formability before final shape forming and application is limited somewhat. Therefore, grain refinement and overall quality improvement during twin-roll casting is of paramount importance. The current work was carried out with a focus on the impact of the as-cast microstructures on the downstream processing of twin-roll cast strip. Research on the downstream processing of magnesium alloy twin-roll cast strip has been focused mainly on grain refinement, texture improvement, and mechanical property measurement.<sup>[19,35,36]</sup> Different combinations of hot and warm rolling have been employed to introduce more shear deformation to alleviate basal texture or to introduce more stored energy at lower temperatures before hot rolling to enhance recrystallization.<sup>[37,38]</sup> Differential speed rolling has also been used for this purpose.<sup>[39,40]</sup> In most cases, the detailed processing conditions are not reported and the main features of the as-cast structures are overlooked. In particular, the evolution of the as-cast columnar dendrite grains and centerline segregation have not been given sufficient attention, which can lead to the formation of a heterogeneous microstructure, voids, and cracks, resulting in premature failure in tensile testing.<sup>[20,41–43]</sup> The current investigation was, therefore, carried out to gain a comprehensive understanding of the principles that govern the mechanical and microstructural behavior of magnesium alloy AZ31 during homogenization, rolling, annealing, and tensile testing for strip produced by the melt-conditioned twin-roll casting and strip produced without the melt-conditioning treatment.

## II. EXPERIMENTAL DETAILS

### A. Twin-Roll Casting

A commercial AZ31 magnesium alloy (Mg–3.34Al–0.97Zn–0.31Mn, wt pct), supplied by Magnesium Elektron (Manchester, UK), was used in this investigation. The alloy was melted in 10-kg batches in a steel crucible at 943 K (670 °C) under a protective atmosphere of nitrogen containing 0.4 vol pct SF<sub>6</sub>. The alloy melt was then transferred to a melt-conditioning unit and subjected to intensive shearing at approximately ~918 K (~645 °C) for 60 seconds. A screw rotation speed of 600 rpm was used, resulting in a melt shear rate of ~1633 seconds<sup>-1</sup>.<sup>[44]</sup> The conditioned liquid was fed immediately into a horizontal twin-roll casting machine under the same protective atmosphere used for melting. The twin-roll caster had a pair of equal-diameter steel rolls of 318 mm diameter and 350 mm width, that can produce 2- to 8-mm-thick strip with a width of ~100 mm. The strip thickness was fixed to ~6 mm and a constant casting speed of 22.5 mm seconds<sup>-1</sup> was employed. For comparison, twin-roll casting was also carried out under similar conditions using the AZ31 alloy melt, but without the melt conditioning process.

### B. Downstream Processing and Mechanical Testing

The AZ31 alloy strips produced using the melt-conditioned twin-roll casting (MCTRC) and by a conventional twin-roll casting (TRC) process were processed by homogenization treatment, hot rolling, and annealing during and after hot rolling to give a final thickness of 1.6 mm before tensile testing. The homogenization treatment was undertaken in air at 623 K, 643 K, 673 K, and 723 K (350 °C, 370 °C, 400 °C, and 450 °C) for various times up to 6 hours, using carbon powder on the surfaces of the samples for protection from oxidation. The samples homogenized at 673 K (400 °C) for 1 hour were hot rolled at a speed of 190 mm seconds<sup>-1</sup> at 673 K (400 °C). The final thickness of 1.6 mm after a total rolling reduction of 73 pct was achieved by nine passes, with an approximately equal reduction of 14 pct for each pass. The strip samples were heated at 673 K (400 °C) for 15 minutes between each pass to restore the strip temperature and the ductility of the material.

An annealing treatment at 623 K (350 °C) for 2 hours was given to the hot-rolled (73 pct reduction) strip, from which ASTM standard tensile samples with a gauge length of 25 mm were prepared parallel to the rolling direction. Tensile tests were carried out on a Lloyd Instrument EZ50 machine (Lloyd Instruments, West Sussex, UK) at room temperature and at a strain rate of  $6.7 \times 10^{-4}$  seconds<sup>-1</sup>.

### C. Microstructure and Texture Characterization

The specimens for the microstructure and texture characterization were cut from the middle of the strip along the casting or rolling direction, and all examinations were carried out on the longitudinal plane or ND-RD/CD plane, where ND stands for normal direction, RD rolling direction and CD casting direction, as shown in Figure 1. The specimens for optical microscopy were prepared using standard metallographic procedures followed by etching in a solution of 5 pct HNO<sub>3</sub> in ethanol. An acetic-picric acid color etching solution, comprising 4.2 g picric acid, 70 mL ethanol, 15 mL distilled water, and 15 mL (concentration) acetic acid, was employed for the preparation of samples to be examined under polarized light. Electropolishing at 12 V in a solution of 15 pct nitric acid in ethanol at 243 K (–30 °C) for 15 seconds was used to prepare surfaces for scanning electron microscopy (SEM) and electron backscatter diffraction (EBSD). The optical microscopic observations and analyses (meaning) were performed on a Carl Zeiss AXioskop 2MAT optical microscope (Carl Zeiss LLC, Chester, VA) equipped with image analysis software. SEM imaging and chemical analysis were carried out on a Zeiss Supera 35 field-emission gun (FEG) scanning electron microscope equipped with an energy dispersive spectroscopy (EDS) facility, and EBSD was carried out using a CamScan MX2000 (CamScan, Cambridgeshire, UK) equipped with an Oxford Instruments HKL EBSD system (Oxford Instruments, Oxfordshire, UK). The measured EBSD data, from which texture information was also obtained, were analyzed using the Oxford Instruments Channel 5 software.

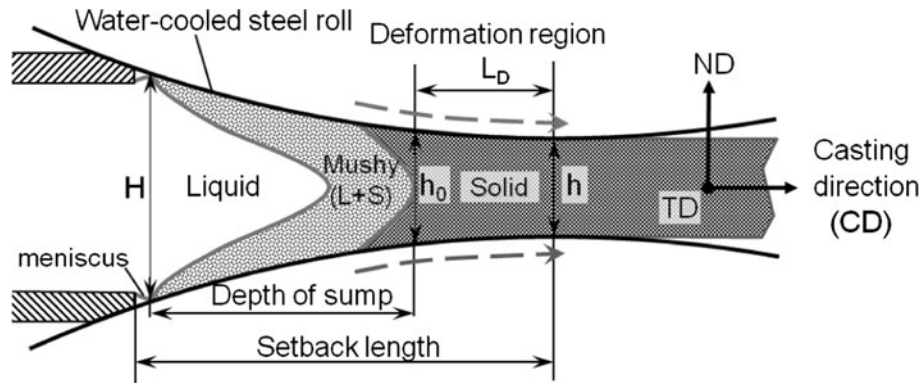


Fig. 1—Schematic diagram of the twin-roll casting process, showing the meniscus points, the profiles of the liquid ( $L$ ), two-phase mushy zone ( $L + S$ ), and solid ( $S$ ) regions and the length of deformation region ( $L_D$ ) in relation to the roll gap in a twin-roll caster.

### III. RESULTS

#### A. The As-Twin-Roll Cast Microstructures

Typical optical micrographs of the microstructures obtained by MCTRC and TRC are shown in Figure 2. The polarized-light micrographs (Figures 2(a) and (c)), which include approximately one half of the strip thickness, show that the microstructure produced by MCTRC is uniform, significantly refined, and almost equiaxed throughout the cross section. In contrast, the TRC microstructure is dominated by a coarse columnar dendrite structure with large, equiaxed grains in the center and a thin, fine-grain chill layer at the surface. The average grain size of the MCTRC strip was approximately  $74\ \mu\text{m}$ , compared with  $616\ \mu\text{m}$  for the TRC strip. Extensive microstructural examination revealed that the MCTRC strip was free from severe centerline segregation, whereas macrosegregation was found at most of the centerline of TRC strip (arrow S in Figure 2(c)). The MCTRC strip also displayed a smaller secondary dendrite arm spacing (SDAS) than the TRC strip. The average grain size, SDAS and their through strip thickness variation were measured, using the mean linear intercept method, with the results given in Table I.

The grain size was measured using polarized-light micrographs with strong orientation contrast, and the SDAS was determined from secondary electron images obtained using the in-lens detector.

More plastic deformation had taken place in the MCTRC strip than in the TRC strip. As a result, the grains in the MCTRC strip were elongated collectively in the CD direction as shown in Figure 2(b). The plastic deformation in the TRC strip occurred mainly in the surface and center regions where grains were elongated slightly (Figures 2(c) and (d)). In the coarse columnar structure, plastic deformation occurred mostly by macroscopic shear banding as shown in Figure 2(d) (arrows A and B).

An additional benefit of the MCTRC process was the refining of  $\beta$ -phase ( $\text{Mg}_{17}\text{Al}_{12}$ ) intermetallic compounds. Figure 3 shows backscattered electron images taken from both MCTRC and TRC samples after electropolishing for 30 seconds (double the normal 15 seconds),

which resulted in preferred dissolution of the  $\alpha$ -magnesium in the eutectic structure, revealing the  $\beta$ -phase network. It can be observed that the  $\beta$ -phase network is consistent with the dendritic structure of the TRC strip, whereas finer and more randomly distributed  $\beta$ -phase particles formed in the MCTRC strip because of the increased severe plastic deformation.

#### B. Homogenization Behavior

During homogenization of an as-cast AZ31 alloy, highly concentrated solute elements, mainly aluminum, in the eutectic structure at interdendritic spaces diffuse into the matrix, and thus, microsegregation is reduced and eventually removed. The MCTRC strip had a substantially higher rate of solute homogenization compared with the TRC strip and also significantly accelerated static recrystallization. The EDS analysis showed that the average aluminum microsegregation amplitude for the MCTRC strip was reduced by approximately 90 pct (from the as-cast 5.52 pct to 3.56 pct, average concentration 3.34 pct) after 1 hour of homogenization at 673 K ( $400\ ^\circ\text{C}$ ) but that 6 hours were required to achieve approximately the same level of reduction for the TRC strip. This can be explained partly by the relatively higher initial microsegregation level (6.27 pct on average) and larger SDAS for the TRC strip. The finer and more uniform microstructure in the MCTRC strip provided more grain boundaries, which is considered to have assisted the homogenization of aluminum levels.

The increased amount of plastic deformation during MCTRC promoted static recrystallization during homogenization, resulting in further grain refinement. For the MCTRC strip, recrystallization started within 10 min and most recrystallized grains were initiated from the existing grain boundaries, forming a typical necklace structure (Figure 4(a)). As homogenization continued, additional grains formed in regions away from grain boundaries, and the recrystallized grains grew at the same time. A recrystallization volume fraction of 72 pct was obtained after 1 hour (Figure 4(b)), and homogenization for 1.5 h resulted in more recrystallized grains but extensive grain growth took place.



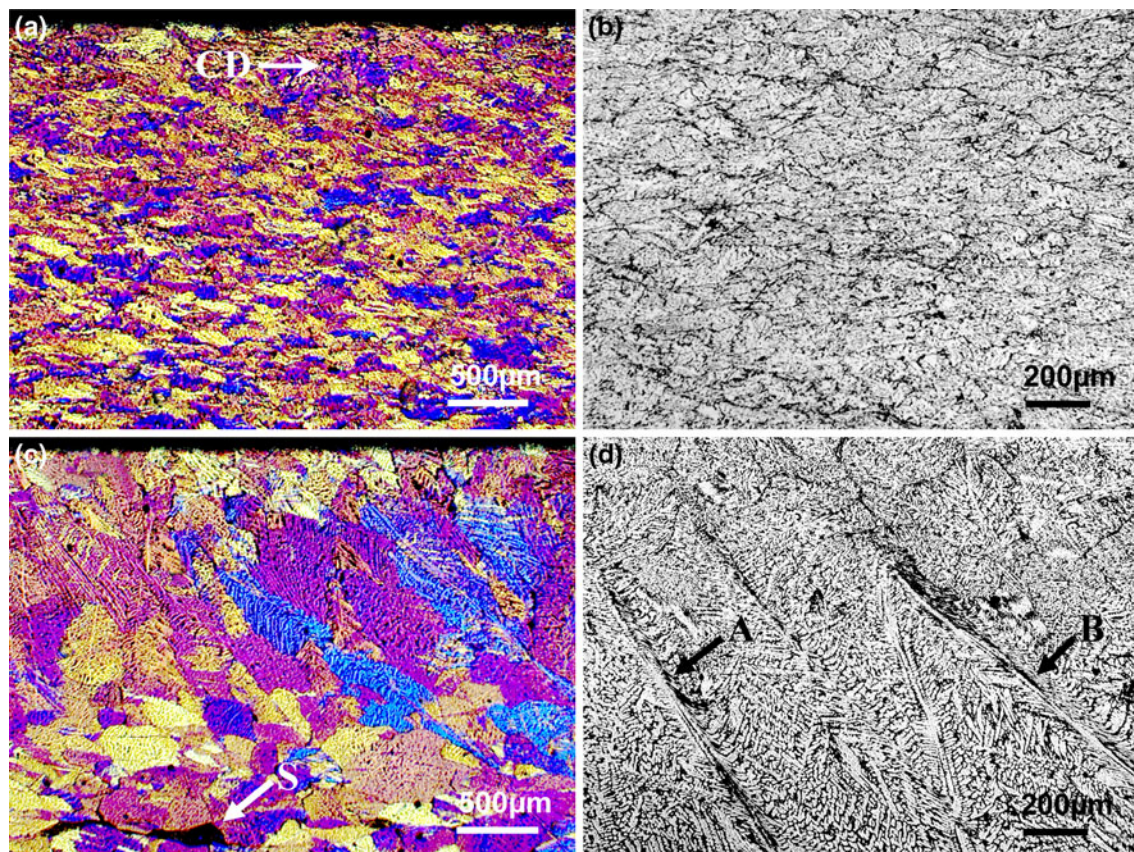


Fig. 2—Optical micrographs of the as-cast microstructures produced by MCTRC (a) and (b), and by TRC (c) and (d); the polarized light micrographs (a) and (c) are presented to show grain structures and the black and white micrographs (b) and (d) to show features of plastic flow.

**Table I. The Microstructural Parameters of the As-Cast State in Both MCTRC and TRC Strips**

	SDAS ( $\mu\text{m}$ )				Grain Size ( $\mu\text{m}$ )			
	Average	Surface	¼ Thickness	½ Thickness	Average	Surface	¼ Thickness	½ Thickness
MCTRC	4.97	$4.94 \pm 0.17$	$5.06 \pm 0.15$	$4.91 \pm 0.19$	74.0	$65.4 \pm 2$	$75.0 \pm 4.2$	$86.4 \pm 4.9$
TRC	8.56	$7.84 \pm 0.1$	$9.21 \pm 0.13$	$8.63 \pm 0.13$	616.0	$380 \pm 25$	$800.0 \pm 42$	$500.0 \pm 25$

For the TRC strip, the recrystallized volume fraction was below 10 pct after 1 hour (Figure 4(c)) and reached only approximately 15 pct after 6 hours of homogenization at 673 K (400 °C) (Figure 4(d)). The recrystallization volume fraction measured for both TRC and MCTRC strip is plotted against time in Figure 5(a), in which the grain size change during homogenization of the MCTRC samples is included, showing a reduction in grain size from the as-cast  $\sim 75 \mu\text{m}$  to  $\sim 12 \mu\text{m}$  after 1 hour of homogenization at 673 K (400 °C). The grain size distribution evolved during homogenization, and Figure 5(b) presents the grain size for both the MCTRC and TRC strips after 1 hour of homogenization at 673 K (400 °C).

### C. Microstructure and Texture Evolution During Hot Rolling and Annealing

The rolling performance of the MCTRC strip was noticeably better than the TRC strip in terms of both

surface finish and the reduced number of cracks and tears at strip edges, suggesting a significant improvement in ductility. In terms of material flow and microstructure evolution, the MCTRC strip was uniform. Figure 6 shows optical micrographs taken from both MCTRC and TRC strip hot-rolled at 673 K (400 °C) to different strains, revealing the overall and representative microstructural features. It can be observed from Figures 6(a) through (d) that the MCTRC microstructure is uniform through the strip thickness, and this uniformity remained for the whole rolling process, although detailed measurements revealed that there was slightly more grain refinement with increased strains as well as an improved distribution of grain size. The grain refinement was attributed mainly to dynamic recrystallization during rolling, and twinning was also found to have an important role. For the TRC strip, both dynamic recrystallization and twinning occurred more intensely than for the MCTRC strip because of the coarse and heterogeneous initial microstructure.



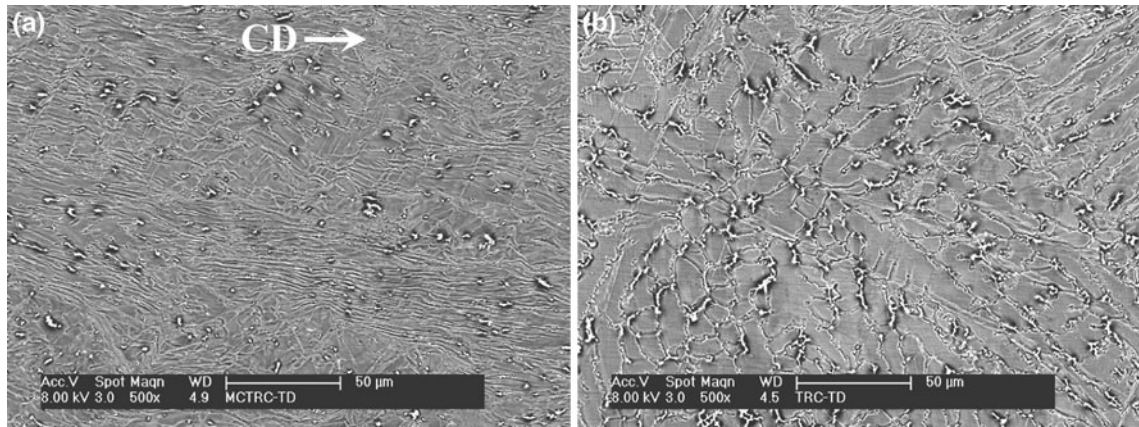


Fig. 3—FEGSEM electron backscattered images, showing microbands formed from the plastic deformation and  $\beta$ -phase size, and the distribution for (a) MCTRC and (b) TRC.

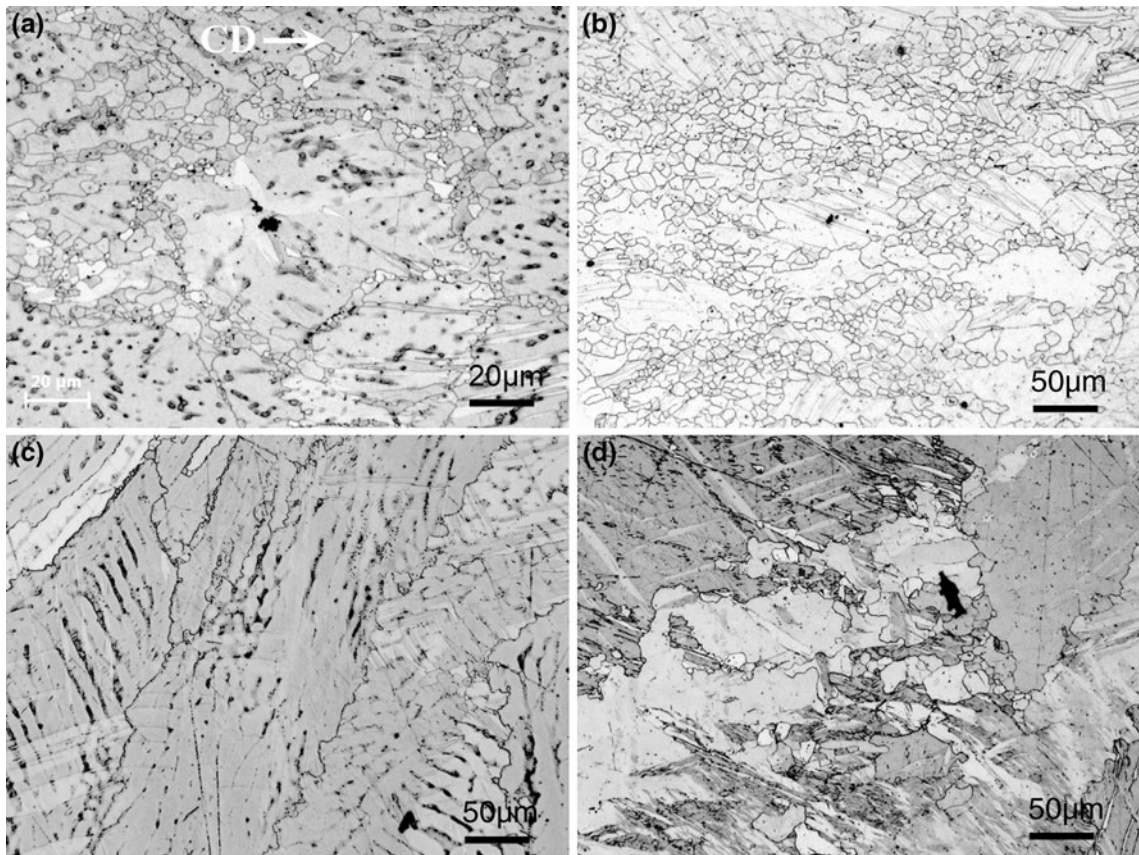


Fig. 4—Optical micrographs showing microstructural features during homogenization at 673 K (400 °C) for MCTRC for (a) 10 min and (b) 1 h, and for TRC for (c) 1 h and (d) 6 h.

Dynamic recrystallization initiated, as usual, in regions around the preexisting grain boundaries and the recrystallized fine grains developed with increased strain, forming a large necklace network on the initial coarse grains as shown in Figures 6(e) through (h). Twinning occurred heavily within large grains and subdivided them into irregular slices. Thus, the grain size in the TRC strip was rapidly refined with increased strain (Table II) compared with the slight decrease in the MCTRC strip.

The data from the homogenized (673 K [400 °C], 1 hour) and annealed (623 K [350 °C], 2 hours after hot rolling) are also included.

However, a uniform grain structure was not obtained for the TRC strip after 73 pct reduction and many grains were still elongated with a wide range of sizes as shown in Figure 6(h). Grain size distributions were determined for both MCTRC and TRC strips as a function of rolling reduction, with the data for 24 pct

and 73 pct reduction shown in Figure 7. Clearly, the narrow, log-normal grain size distribution developed in the MCTRC strip is advantageous over the scattered and bimodal distribution of the TRC strip.

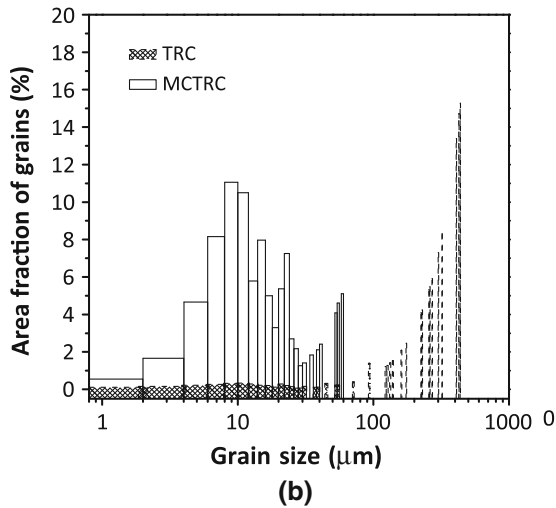
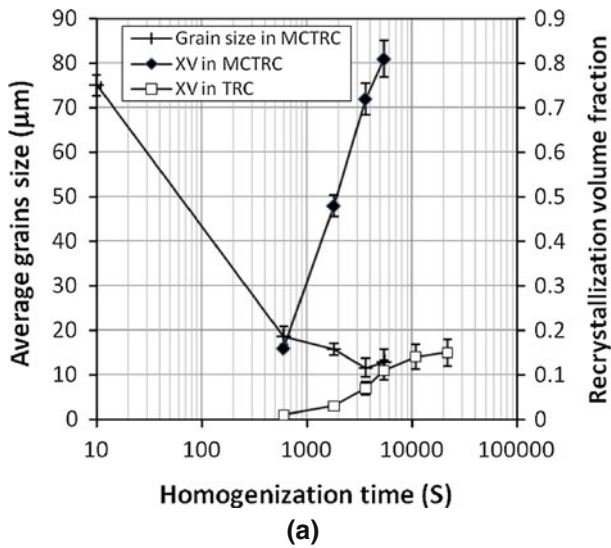


Fig. 5—Characteristic features of microstructural evolution during homogenization at 673 K (400 °C): (a) The volume fraction of recrystallization as a function of homogenization time (MCTRC grain size included) and (b) grain size distribution after 1 h homogenization.

The hot rolled MCTRC and TRC strips were annealed at 623 K (350 °C) for 2 h, with the resultant microstructures displayed in Figure 8. It can be seen that twins are removed and grain boundaries are smoothed with more equilibrium triple junctions. There was a slight increase in the average grain size (Table II), but the grain size distribution did not change significantly compared with that shown in Figure 7.

The textures developed in the as-cast, hot rolled and the annealed states were obtained by EBSD, with the results summarized in Table III.

As expected, the {0001} basal texture dominated in the as-cast, as-hot-rolled, and after the final annealing following hot rolling. A weak {10-10}{11-20} component was found in the as-cast state for both MCTRC and TRC strips, which remained after hot rolling but not after annealing. This {10-10}{11-20} component could be caused by either {10-12} twinning or the operation of the prismatic {10-10}{11-20} slip systems. EBSD examination showed that it was most likely caused by twinning. Overall, it is evident from Table III that the texture intensity and components show limited differences between the MCTRC and TRC strip.

#### D. Mechanical Properties

Tensile testing of the hot-rolled and annealed strips was carried out to examine their mechanical properties and to provide an estimate of their formability. Figure 9 shows typical tensile stress–strain curves of both MCTRC and TRC samples. It can be observed that the MCTRC sample had a remarkably high tensile elongation of ~28 pct, in comparison with ~9 pct for the TRC strip and the reported data of 6 to 16 pct for the alloys prepared by other processes.<sup>[18,45–48]</sup> Five samples were tested for each condition, and the averaged results are given in Table IV.

The material produced by MCTRC also showed excellent features of yield and failure. As shown in the inset in Figure 9, in which the stress–strain curves in the yield region are magnified, the TRC sample had an apparent yield point. Conversely, the MCTRC sample exhibited a smooth and gradual start of plastic flow, indicating that there was no apparent strain instability in the early stages of plastic deformation. In terms of failure, all the TRC strip samples failed by brittle

Table II. Grain Size and Volume Fraction of Recrystallization as a Function of Hot-Rolling Strain in Both MCTRC and TRC Strips

	Homogenized (1 h, 673 K [400 °C])	24 pct Hot Rolled	41 pct Hot Rolled	59 pct Hot Rolled	73 pct Hot Rolled	Annealed (73 pct Hot Rolled + 623 K [350 °C] 2 h)
Mean grain size (μm)						
MCTRC	11.6 ± 1	11.3 ± 0.7	10.1 ± 0.8	8.7 ± 0.4	8.4 ± 0.4	9.5 ± 0.5
TRC	313 ± 10	141.6 ± 10	112 ± 8	56.3 ± 4	32.1 ± 5	36.4 ± 3
REX grain size (μm)						
MCTRC	11.3 ± 0.4	10.4 ± 0.2	9.1 ± 0.4	8.2 ± 0.3	—	9.5 ± 0.5
TRC	13.5 ± 0.8	12.5 ± 0.3	11.6 ± 0.5	11.4 ± 0.2	11.8 ± 0.2	12.2 ± 0.4
Fraction of REX (pct)						
MCTRC	72 ± 3.1	—	—	—	—	100
TRC	3.1 ± 0.7	15.5 ± 1.4	59.0 ± 4.8	67.4 ± 5.4	70.0 ± 6.3	75.1 ± 6.4



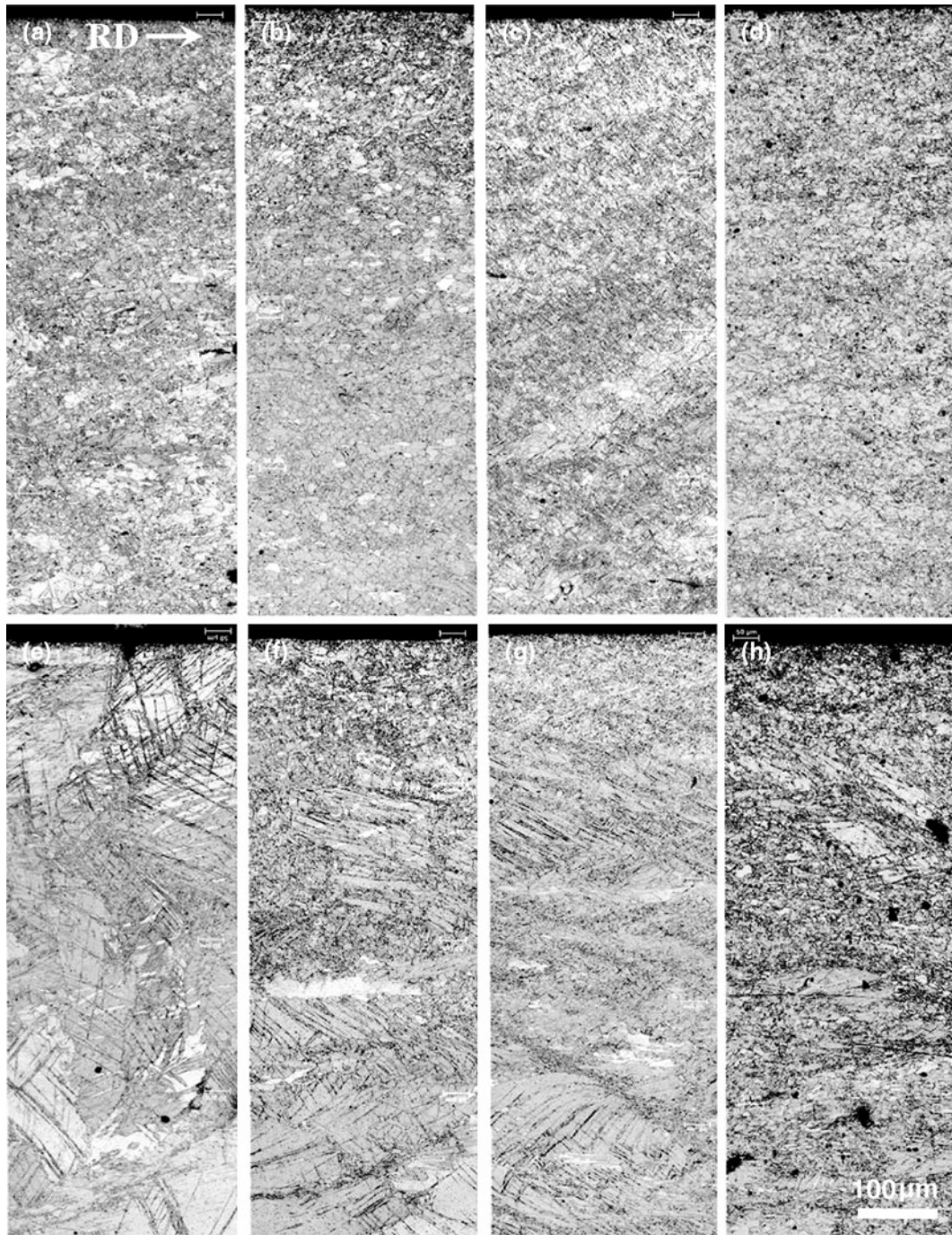


Fig. 6—Optical micrographs showing the microstructures obtained after hot rolling at 673 K (400°C) to various reductions for MCTRC (*a*) 24 pct, (*b*) 41 pct, (*c*) 59 pct, and (*d*) 73 pct and for TRC (*e*) 24 pct, (*f*) 41 pct, (*g*) 59 pct, and (*h*) 73 pct.

fracture and little plastic flow occurred before rupture, whereas the MCTRC strip samples failed by ductile fracture, with significant necking before failure.

#### IV. DISCUSSION

The most important effect of melt conditioning by intensive shearing is the dispersion of the oxide particles present in the alloy melt.<sup>[26]</sup> These oxide particles then act as potent nucleating sites to enhance

heterogeneous nucleation during solidification, which has been confirmed experimentally.<sup>[26]</sup> The current experimental results showed clearly that the melt conditioning technique prior to TRC improved the overall quality of the resultant AZ31 magnesium alloy strip substantially. The results revealed also that the refined and uniform microstructure of the MCTRC strip had a strong, positive influence on downstream processing and mechanical properties at final gauge. The following discussion focuses on the solidification behavior and the effect of the refined and uniform

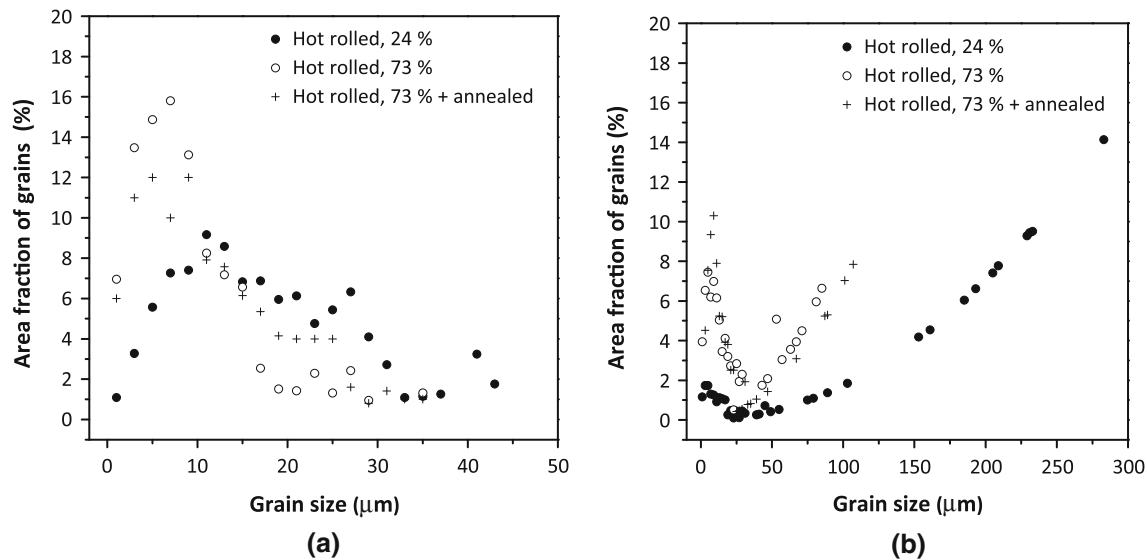


Fig. 7—Grain size distribution after hot rolling at 673 K (400 °C) to 24 pct and 73 pct, and after annealing at 623 K (350 °C) for 2 h for (a) MCTRC and (b) TRC.

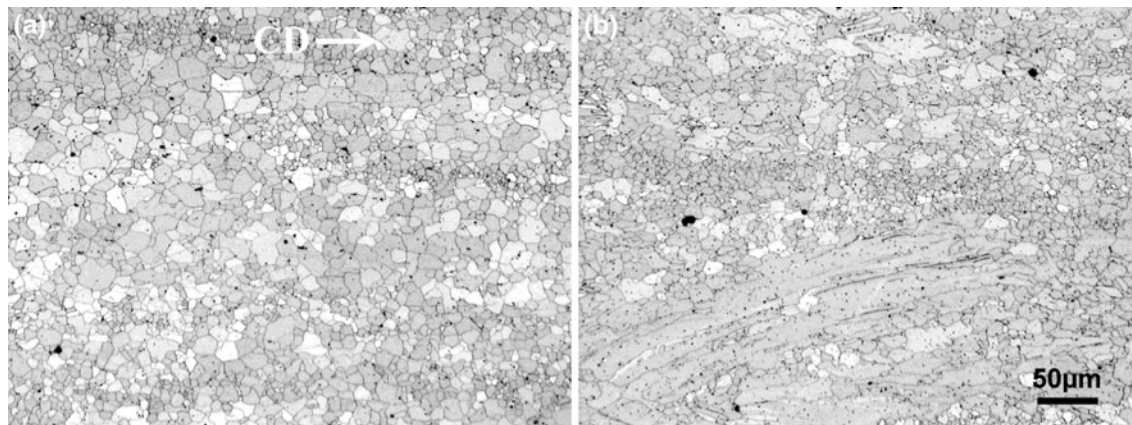


Fig. 8—The microstructures after annealing at 623 K (350 °C) for 2 h (after hot rolling to 73 pct at 673 K [400 °C]) for (a) MCTRC and (b) TRC.

microstructure on the downstream processing and mechanical properties.

#### A. The Formation of the As-Cast Microstructures

A conservative estimate of the mean true strain:  $\varepsilon = \ln \sqrt{\psi}$  can be made from the average grain aspect ratio ( $\psi$ ) (grain size in CD/grain size in ND) because the grain elongation in the CD direction can only be caused by the rolling plastic deformation. For the MCTRC strip,  $\psi$  was measured as  $\sim 1.94$  and  $\varepsilon \approx 0.33$ , which is equivalent to a rolling reduction of 28 pct. For the TRC strip, the rolling reduction was approximately 17 pct for the surface and center regions, and the average value was 14 pct. The length of plastic deformation region ( $L_D$ ) (Figure 1) is related to the rolling strain ( $\varepsilon_e$ ) by  $L_D = \sqrt{\varepsilon_e h D} / (1 - \varepsilon_e)$ , where  $h$  is the strip thickness after casting and  $D$  is the diameter of the caster rolls. The enhanced heterogeneous nucleation caused by melt

conditioning in the MCTRC resulted in a nearly doubled  $L_D$  of 31.9 mm compared with 18.9 mm for TRC. This effectively reduced the sump depth of the solidification zone, which is considered to be the key reason for the elimination of severe centerline segregation.

Grain size is determined essentially by the competition between nucleation rate and growth velocity, whereas SDAS ( $\lambda$ ) is related largely to the dynamic response of the alloy to the solidification conditions. SDAS is also an important parameter for characterizing solidification microstructures because it is related to the severity of microsegregation and various other casting defects. According to Feurer and Wunderlin<sup>[49]</sup>

$$\lambda = 5.5 \left( \frac{\Delta T_0 M}{G_L R} \right)^{1/3} \quad [1]$$

where  $\Delta T_0$  is the temperature range in the two-phase (L + S) region of the alloy,  $G_L$  is the temperature



**Table III. Texture Components (within  $\pm 10^\circ$  of Ideal Orientations) and Their Average Maximum Intensity (Times of Random) Measured by EBSD Over Three or More Maps Obtained on Representative Areas of  $500 \times 500 \mu\text{m}^2$  or Larger in Both MCTRC and TRC Strips**

	{0001} <sup>*</sup> Basal	{0001} (11-20)	{0001} (10-10)	{10-10} (11-20)
As-cast				
MCTRC	6.43	—	—	2.84
TRC	4.55	—	—	1.71
Hot rolled 73 pct				
MCTRC	11.33	(2.76)	(1.58)	3.91
TRC	12.5	—	—	1.95
Annealed				
MCTRC	10.84	(2.47)	—	—
TRC	10.06	—	—	—

<sup>\*</sup>Including {0001}(11-20) and {0001}(10-10) components.

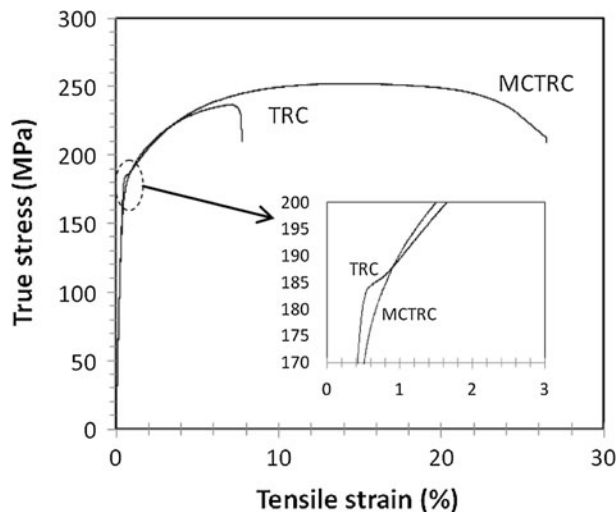


Fig. 9—Typical tensile testing stress–strain plots for the MCTRC and TRC strip after processing (homogenization at 673 K [400 °C] for 1 h, hot rolling at 673 K [400 °C] to 73 pct reduction, and annealing at 623 K [350 °C] for 2 h). The inserted diagram shows the different yielding response of samples for the MCTRC and TRC strip.

gradient in the liquid,  $R$  is the solid–liquid interface velocity, and  $M$  is a material and compositional concentration determined parameter. The differences in the SDAS values between the MCTRC and TRC strips, with an upper-bound estimate of 25 pct, may be explained partly by the difference in plastic flow, which has an effect of compressing the dendrite arms in proportion to the amount of reduction. Most of the reduced SDAS in the MCTRC is caused most likely by the change of solidification conditions as indicated by Eq. [1]. If the changes in  $\Delta T_0$  and  $M$  are negligible, which is reasonable for the same alloy, only the increase in the temperature gradient in the liquid ahead of the liquid–solid interface  $G_L$  and/or the solid–liquid interface velocity  $R$  would lead to a reduction in SDAS as suggested by Eq. [1]. The clear indication from this analysis is that melt conditioning not only enhances heterogeneous nucleation but also improves solidification kinetics.

### B. Accelerated Homogenization

According to Porter and Easterling,<sup>[50]</sup> if the concentration ( $C$ ) of a solute element maximized ( $\beta_0$ ) at the interdendrite region and minimized at the same amplitude of  $-\beta_0$  in the centre of the dendrite arms, which has an average spacing of  $\lambda$ , has a sinusoidal distribution  $C = C_0 + \beta_0 \sin(\pi x/\lambda)$ , where  $C_0$  is the average concentration. The amplitude of the concentration profile ( $\beta$ ) after a time ( $t$ ) is given by  $C$  at  $x = \lambda/2$ , i.e.,

$$\beta = \beta_0 \exp\left(-\frac{\pi^2 D t}{\lambda^2}\right) \quad \text{or} \quad t = \frac{\lambda^2}{\pi^2 D} \ln \frac{\beta_0}{\beta} \quad [2]$$

This equation indicates that the time required to obtain a certain level of homogenization ( $\beta/\beta_0$ ) is proportional to  $\lambda^2$ . According to Eq. [2], the difference in the measured SDAS between MCTRC and TRC microstructures should result in a factor of three difference in the homogenization speed. However, the actual difference was more than six times according to the EDS analysis results. The refined cast microstructure of the MCTRC strip and its subsequent refinement by static recrystallization during homogenization is also considered to be a factor enhancing the homogenization rate, as the fine grain structure provided shorter paths for the diffusion of the segregated aluminum. For the current analysis,  $D$  in Eq. [2] should be taken as an effective diffusion coefficient:  $D = fD_{gb} + (1-f)D_l$ , where  $D_{gb}$  is the grain boundary diffusion coefficient,  $D_l$  the lattice diffusion coefficient, and the partition constant  $f$  can be estimated by  $f = \delta q/d$ , where  $q$  is the value based on grain shape between 1 for lamellar grains and 3 for ideal equiaxed grains,  $d$  is the average grain size and  $\delta$  is the grain boundary width, taken to be 0.5 nm as usual.<sup>[51]</sup> At 673 K (400 °C),  $D_l = 1.2 \times 10^{-3} \exp(-143,000/8.314/673) \text{ m}^2\text{s}^{-1}$  and  $D_{gb} = 1 \times 10^{-2} \exp(-92,000/8.314/673) \text{ m}^2\text{s}^{-1}$ ,<sup>[52–54]</sup> giving  $D_{gb}/D_l \approx 7.5 \times 10^4$ . Because the grain boundary diffusion coefficient is inversely proportional to the average grain size, the grain boundary diffusion ( $fD_{gb}$ ) becomes dominating over lattice diffusion ( $(1-f)D_l$ ) when the grain size changes from 100  $\mu\text{m}$  ( $f = 1 \times 10^{-5}$ ) to 10  $\mu\text{m}$  ( $f = 1 \times 10^{-4}$ );  $q$  is taken as 2 in the estimates of  $f$ .

**Table IV. Room-Temperature Tensile Properties of the MCTRC and TRC Strips after Homogenization at 673 K (400 °C) for 1 h, Hot Rolling at 673 K (400 °C) to 73 pct and Annealing at 623 K (350 °C) for 2 h**

	Yield Stress (MPa)	UTS (MPa)	Uniform Elongation (pct)	Elongation to Fracture (pct)
MCTRC	177.7 ± 3.3	251.1 ± 2.1	14.6 ± 0.27	27.7 ± 2.1
TRC	181.6 ± 1.9	243.1 ± 2.7	6.1 ± 0.45	9.6 ± 0.7

It is then clear that the average grain size of between ~75  $\mu\text{m}$  and ~12  $\mu\text{m}$  for the MCTRC strip should have allowed grain boundary diffusion to control homogenization and accelerated kinetics to occur.

Melt conditioning by intensive shear both refines microstructure during casting and accelerates homogenization by providing more grain boundary paths for the diffusion of solute.

### C. Static Recrystallization During Homogenization

The static recrystallization of the MCTRC strip benefited from the more severe plastic deformation and therefore higher stored energy. This recrystallization resulted in a further refined microstructure. For the TRC microstructure, recovery dominated the process of the release of the stored energy. The recrystallization kinetics shown in Figure 5(a) were fitted to the JMAK model  $X_v = 1 - \exp(-Bt^n)$ , where  $X_v$  is recrystallization volume fraction, and  $B$  and  $n$  are constants. The constant  $n$  or the Avrami exponent was determined from the slope of the  $\ln(1/(1 - X_v))$  vs  $\ln t$  plots (Figure 10(a)) to be ~1.15 for both MCTRC and TRC data, indicating that the two types of microstructures shared the same recrystallization kinetics. The Avrami exponent of 1.15 is close to the result ( $n = 1.27$ ) obtained from kinetic measurements during the postdeformation recrystallization of the same alloy by Beer and Barnett,<sup>[55]</sup> suggesting that the nature of the recrystallization during homogenization after TRC is similar to that after normal plastic deformation. The annealing temperature has a strong effect on the recrystallization kinetics. The time for 50 pct recrystallization ( $t_{0.5}$ ) is often used as a measure of the rate of recrystallization, and its dependency on temperature is given by  $t_{0.5} = A \exp(Q/RT)$ , where  $A$  is a constant,  $Q$  is the process activation energy, and  $R$  and  $T$  have their usual meanings.  $t_{0.5}$  was measured over a range of temperature from 623 K to 723 K (350 °C to 450 °C) and is plotted against  $1/T$  in Figure 10(b). It can be observed that there is a good straight line fit between  $1/T$  and the logarithmic scale of time; the activation energy of the recrystallization, determined from the slope of the straight line, was 141 kJ mol<sup>-1</sup>. Although it is difficult to interpret this value because it refers to the transformation as a whole without differentiating nucleation and growth, its closeness to the activation energy for aluminum diffusion in magnesium<sup>[52,53]</sup> suggests strongly the importance of aluminum diffusion in the process.

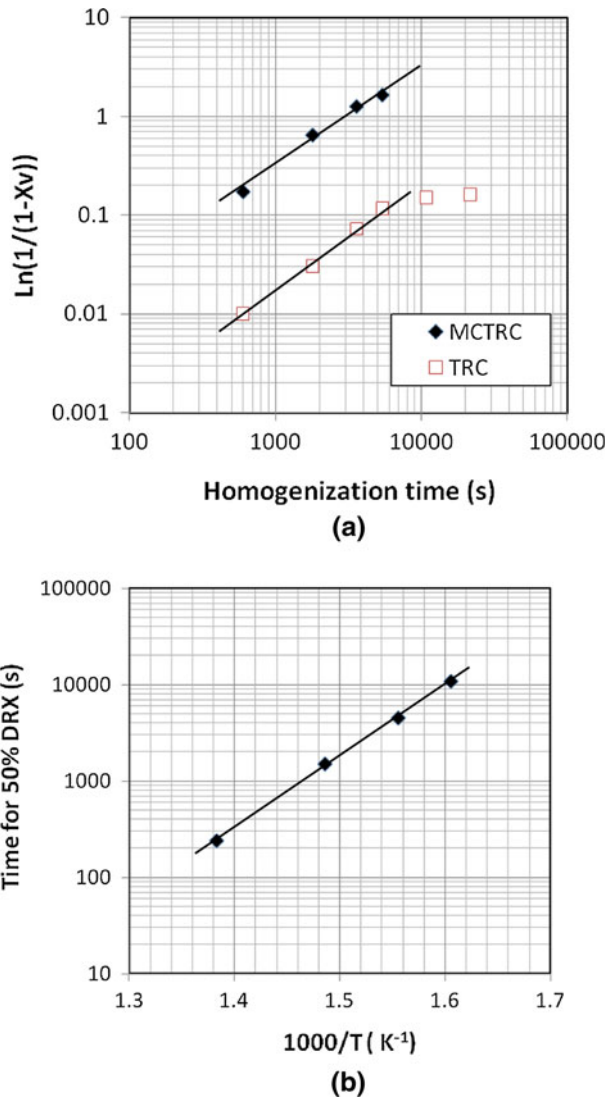


Fig. 10—Analysis of static recrystallization during homogenization: (a) volume fraction of recrystallization as a function of homogenization time at 673 K (400 °C) and (b) the time for 50 pct recrystallization volume fraction as a function of temperature for the MCTRC strip.

### D. Dynamic Recrystallization During Hot Rolling

The TRC strip displayed typical dynamic recrystallization features<sup>[56]</sup> that were characteristic of coarse grained magnesium alloys, as shown in Figures 6(e) through (h). Subsequent microscopy revealed that the mechanisms of nucleation include discontinuous nucleation in shear bands (arrows SB1 and SB2 in



Figure 11(c)), primary twin boundaries (arrow PT in Figure 11(c)), and secondary twin boundaries (arrow ST in Figure 11(c)), as well as continuous and/or discontinuous nucleation along grain boundaries and the twin network (Figure 11(d)). With additional rolling, the recrystallized grains underwent more deformation and more dynamic recrystallization took place around them, resulting in the broadening of the fine grain necklace structure and an increased volume fraction of recrystallization (Figures 6(g) and (h)).

For the MCTRC strip, nucleation from existing grain boundaries was important in the early stage of rolling as displayed in Figure 11(a) (arrows C and D), which shows apparently smaller grains formed around grain boundaries after 24 pct rolling, and twinning was also observed frequently in relatively large grains (arrows T1 and T2 in Figure 11(b)). In the later stages, continuous dynamic recrystallization would be the more likely process for the restoration process during rolling as no obvious new grains were developed and the grain boundaries became smoother. It should be noted that, without generating new grain boundaries, there should be a reduction in grain size along ND corresponding to the plastic strain by a factor of  $\exp(-\epsilon)$ , which is 0.86 between each pass of 14 pct reduction and is approximately 0.25 for the total reduction of 73 pct. However, the grain size actually decreased by a total factor 0.74 after 73 pct rolling and an average factor of 0.9 between

passes. Taking into account that the intermediate heating between passes largely eliminated most of the twins and dislocations and that there was a significant amount of new grain boundaries, including twin boundaries, generated in the material, the results suggest strongly that there was significant dynamic grain growth during deformation that, with the dynamic recrystallization, allowed the fine and uniform grain structure to be maintained through the hot-rolling process.

### E. The Enhanced Mechanical Properties

A microstructural examination showed that the significantly improved tensile properties of the MCTRC strip at final gauge compared with the TRC strip at the same gauge were mainly caused by two reasons: (1) the refined and uniform microstructure and (2) the elimination of severe centerline segregation, which remained in the TRC strip after downstream processing. The size and distribution of intermetallic particles might have had some effect, but clear evidence to support this was not found. Textures usually have a strong effect on the tensile deformation behavior of wrought magnesium alloys,<sup>[48,56–58]</sup> but in this work, the effect was limited because there were little significant differences in the texture components and intensity between the MCTRC and TRC strips.

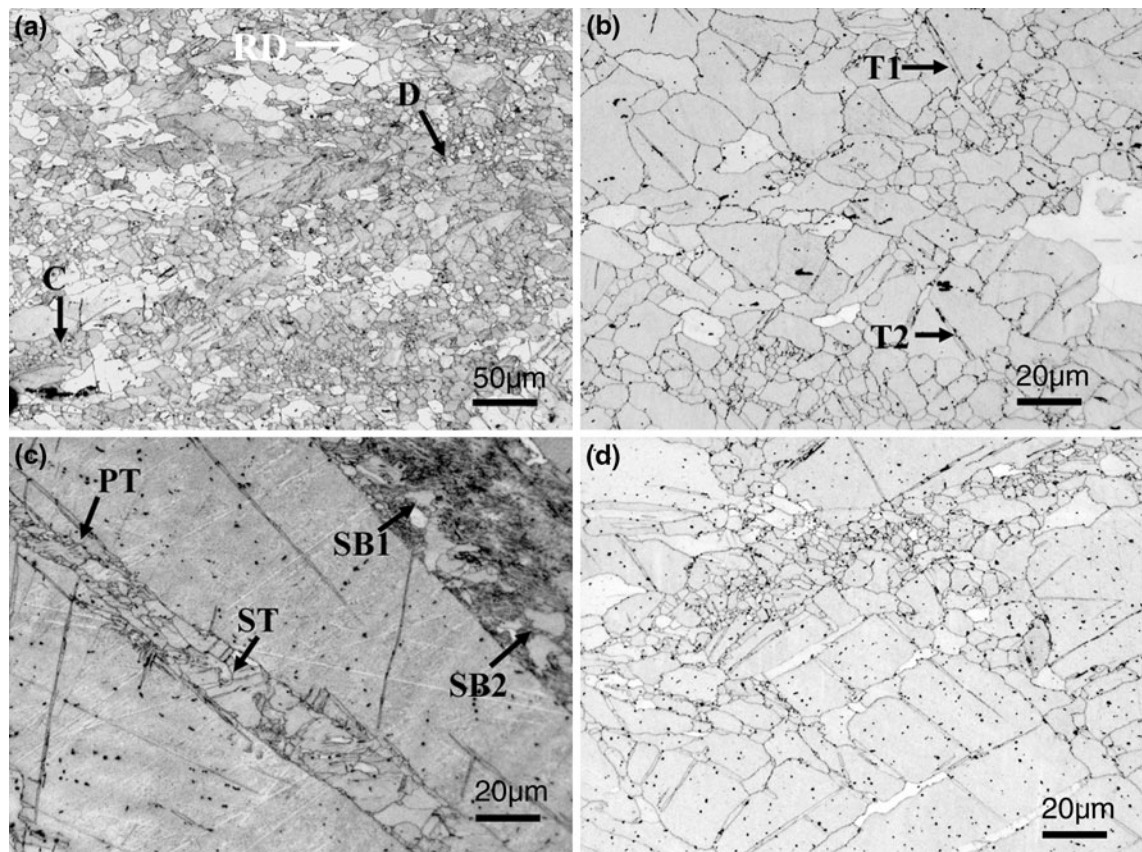


Fig. 11—Optical micrographs showing features of dynamic recrystallization during hot rolling at 673 K (400 °C) to reductions of (a) 24 pct and (b) 41 pct for MCTRC, and (c) 24 pct and (d) 41 pct for TRC.

## V. CONCLUSIONS

1. The application of intensive shearing melt conditioning prior to twin roll casting of an AZ31 magnesium alloy improved substantially the quality of the strip produced by enhancing heterogeneous nucleation of solidification, which resulted in a refined, uniform, and nearly equiaxed microstructure, and the elimination of severe centerline segregation.
2. The refined and uniform as-cast microstructure of the MCTRC strip exhibited significantly accelerated kinetics of homogenization in comparison with the TRC strip, by providing more intergranular paths for diffusion and higher stored energy for transformation.
3. The increased amount of plastic deformation in the MCTRC strip generated higher stored energy in the material and was responsible mainly for the enhanced kinetics of static recrystallization and grain refinement during homogenization, which had a strong influence on the behavior during subsequent processing.
4. During hot rolling, the MCTRC strip showed uniform plastic flow and the fine and uniform microstructure remained and gradually refined through the successive rolling and heating cycles. For the TRC strip, the microstructural evolution was governed by dynamic recrystallization around preexisting grain boundaries, resulting in a partly refined, heterogeneous grain structure.
5. Twinning occurred during casting and hot rolling, and it played an important role in the microstructural development in both MCTRC and TRC strip; the twins generated could be removed by an annealing treatment after hot rolling.
6. The MCTRC strip at final gauge exhibited steady yield behavior and ductile fracture in tensile testing, with a high average elongation of 28 pct, compared with 9 pct for the TRC strip.

## ACKNOWLEDGMENTS

Financial support is acknowledged from Engineering and Physical Sciences Research Council for Brunel and the Manchester LATEST Portfolio Partnership.

## REFERENCES

1. B.L. Mordike and T. Ebert: *Mater. Sci. Eng. A*, 2001, vol. 302, pp. 37–45.
2. I.J. Polmear: *Light Alloys from Traditional Alloys to Nanocrystals*, 4th ed., Elsevier/Butterworth-Heinemann, Oxford, UK, 2006, pp. 1–28.
3. J. Koike, T. Kobayashi, T. Mukai, H. Watanabe, M. Suzuki, K. Maruyama, and K. Higashi: *Acta Mater.*, 2003, vol. 51, pp. 2055–65.
4. A. Galiyev, R. Kaibyshev, and G. Gottstein: *Acta Mater.*, 2001, vol. 49, pp. 1199–1207.
5. S.E. Ion, F.J. Humphreys, and S.H. White: *Acta Metall.*, 1982, vol. 30, pp. 1909–19.
6. J.A. Del Valle, M.T. Pérez-Prado, and O.A. Ruano: *Mater. Sci. Eng. A*, 2003, vol. 355, pp. 68–78.
7. M.R. Barnett: *Mater. Sci. Eng. A*, 2007, vol. 464, pp. 8–16.
8. M. Mabuchi, T. Asahina, H. Iwasaki, and K. Higashi: *Mater. Sci. Technol.*, 1997, vol. 13, pp. 825–31.
9. N. Stanford and D. Phelan: *Acta Mater.*, 2010, vol. 58, pp. 3642–54.
10. A. Yamashita, Z. Horita, and T.G. Langdon: *Mater. Sci. Eng. A*, 2001, vol. 300, pp. 142–47.
11. K. Matsubara, Y. Miyahara, Z. Horita, and T.G. Langdon: *Metall. Mater. Trans. A*, 2004, vol. 35A, pp. 1735–44.
12. Q. Yang and A.K. Ghosh: *Acta Mater.*, 2006, vol. 54, pp. 5147–58.
13. J.A. Del Valle, M.T. Pérez-Prado, and O.A. Ruano: *Mater. Sci. Eng. A*, 2005, vols. 410–411, pp. 353–57.
14. N. Stanford and M.R. Barnett: *J. Alloys Compd.*, 2008, vol. 466, pp. 182–88.
15. E. Essadiqi, M.T. Shehata, A. Javaid, C. Galvani, G. Shen, S. Yue, and R. Verma: *JOM*, 2009, vol. 61, pp. 25–28.
16. S.R. Agnew and Ö. Duygulu: *Int. J. Plast.*, 2005, vol. 21, pp. 1161–93.
17. M.R. Barnett, N. Stanford, P. Cizek, A. Beer, Z. Xuebin, and Z. Keshavarz: *JOM*, 2009, vol. 61, pp. 19–24.
18. R.V. Allen, T.J. Johnson, W.E. Borbidge, and D. Liang: *Magnesium Technology 2001*, J.N. Hryn, ed., TMS, Warrendale, PA, 2001, pp. 75–80.
19. S.S. Park, W.-J. Park, C.H. Kim, B.S. You, and N.J. Kim: *JOM*, 2009, vol. 61, pp. 14–18.
20. M. Ferry: *Direct Strip Casting of Metals and Alloys*, Woodhead Publishing Limited, Cambridge, UK, 2006, pp. 54–58, 101–50, 191.
21. D. Liang and C.B. Cowley: *JOM*, 2004, vol. 56, pp. 26–28.
22. D. Liang, W. Borbidge, D.R. East, and R.V. Allen: US Patent No. 7,028,749 B2, 2006.
23. I. Bayandorian, Z. Bian, M. Xia, H. Zhang, G.M. Scamans, and Z. Fan: *Magnesium Technology 2009*, E.A. Nyberg, S.R. Agnew, N.R. Neelameggham, and M.O. Pekguleryuz, eds., TMS, Warrendale, PA, 2009, pp. 363–68.
24. Z. Fan: *Int. Mater. Rev.*, 2002, vol. 47, pp. 49–85.
25. Y. Mizutani, T. Tamura, and K. Miwa: *Mater. Sci. Eng. A*, 2005, vols. 413–414, pp. 205–10.
26. Z. Fan, Y. Wang, M. Xia, and S. Arumuganathar: *Acta Mater.*, 2009, vol. 57, pp. 4891–4901.
27. D.H. St John, M. Qian, M.A. Easton, P. Cao, and Z. Hildebrand: *Metall. Mater. Trans. A*, 2005, vol. 36A, pp. 1669–79.
28. Y. Wang, X. Zeng, W. Ding, A.A. Luo, and A.K. Sachdev: *Metall. Mater. Trans. A*, 2007, vol. 38A, pp. 1358–66.
29. Z. Fan and G. Liu: *Acta Mater.*, 2005, vol. 53, pp. 4345–57.
30. Y. Wang, G. Liu, and Z. Fan: *Acta Mater.*, 2006, vol. 54, pp. 689–99.
31. S. Ji and Z. Fan: *Metall. Mater. Trans. A*, 2002, vol. 33A, pp. 3511–20.
32. Z. Fan, G. Liu, and Y. Wang: *J. Mater. Sci.*, 2006, vol. 41, pp. 3631–44.
33. Z. Bian, I. Bayandorian, and Z. Fan: *Mater. Sci. Technol.*, 2009, vol. 25, pp. 599–606.
34. I. Bayandorian: Ph.D. Dissertation, Brunel University, UK, 2010.
35. M. Masoumi, F. Zarandi, and M.O. Pekguleryuz: *Scripta Mater.*, 2010, vol. 62, pp. 823–26.
36. H. Chen, S.B. Kang, H. Yu, H.W. Kim, and G. Min: *Mater. Sci. Eng. A*, 2008, vol. 492, pp. 317–26.
37. L. Jin, J. Dong, R. Wang, and L.M. Peng: *Mater. Sci. Eng. A*, 2010, vol. 527, pp. 1970–74.
38. Y. Wang, S.B. Kang, and J. Cho: *J. Mater. Proc. Technol.*, 2010, vol. 210, pp. 1270–75.
39. X. Huang, K. Suzuki, A. Watazu, I. Shigematsu, and N. Saito: *J. Alloys Compd.*, 2009, vol. 470, pp. 263–68.
40. X. Gong, H. Li, S.B. Kang, J.H. Cho, and S. Li: *Mater. Des.*, 2010, vol. 31, pp. 1581–87.
41. J.M. Boileau, P.A. Friedman, D.Q. Houston, and S.G. Luckey: *J. Mater. Eng. Perform.*, 2010, vol. 19, pp. 467–80.
42. S.S. Park, G.T. Bae, D.H. Kang, In-Ho Jung, K.S. Shind, and N.J. Kimb: *Scripta Mater.*, 2007, vol. 57, pp. 793–96.



43. J.P. Weiler, T.J. Wood, R.J. Klassen, E. Maire, R. Berkmortel, and G. Wang: *Mater. Sci. Eng. A*, 2005, vol. 395, pp. 315–22.
44. S. Ji, Z. Fan, and M.J. Bevis: *Mater. Sci. Eng. A*, 2001, vol. 299, pp. 210–17.
45. M.M. Avedesian and H. Baker: *ASM Specialty Handbook: Magnesium and Magnesium Alloys*, ASM, Materials Park, OH, 1999, pp. 12–25, 165–72, 226–48, 258–63.
46. V. Laurent, P. Jarry, G. Regazzoni, and D. Apelian: *J. Mater. Sci.*, 1992, vol. 27, pp. 4447–59.
47. S.F. Hassan and M. Gupta: *J. Alloys Compd.*, 2007, vol. 429, pp. 176–18.
48. M. Paramsothy, S.F. Hassan, N. Srikanth, and M. Gupta: *Mater. Sci. Eng. A*, 2009, vol. 527, pp. 162–68.
49. U. Feurer and R. Wunderlin: *Dtsch. Ges. Metallkd. Fachber.*, 1978, pp. 21–28.
50. D.A. Porter and K.E. Easterling: *Phase Transformation in Metals and Alloys*, 2nd ed., Chapman & Hall, London, UK, 1992, pp. 71–75.
51. P. Heitjans and J. Karger: *Diffusion in Condensed Matter: Methods Materials Models*, 2nd ed., Birkhauser, Basel, Switzerland, 2005, pp. 337–63.
52. A.M. Brown and M.F. Ashby: *Acta Metall.*, 1980, vol. 28, pp. 1085–97.
53. R.B. Figueiredo and T.G. Langdon: *J. Mater. Sci.*, 2008, vol. 43, pp. 7366–71.
54. H.-K. Kim and W.-J. Kim: *J. Mater. Sci.*, 2007, vol. 42, pp. 6171–76.
55. A.G. Beer and M.R. Barnett: *Scripta Mater.*, 2009, vol. 61, pp. 1097–1100.
56. F.J. Humphreys and M. Hatherly: *Recrystallization and Related Annealing Phenomena*, 2nd ed., Elsevier, Amsterdam, the Netherlands, 2004, pp. 67–78, 439.
57. W. Woo, H. Cho, D.W. Brown, P.K. Liaw, and Z. Feng: *Scripta Mater.*, 2006, vol. 4, pp. 1859–64.
58. Z. Zuberova, L. Kunz, T.T. Lamark, Y. Estrin, and M. Janecek: *Metall. Mater. Trans. A*, 2007, vol. 38A, pp. 1934–40.